ADVANCED ELECTRONIC MATERIALS Open Access
www.advelectronicmat.de

Efficient In Situ Doping of Strained Germanium Tin Epilayers at Unusually Low Temperature

Maksym Myronov, Pedram Jahandar, Simone Rossi, Kevin Sewell, Felipe Murphy-Armando, and Fabio Pezzoli*

Efficient p- and n-type in situ doping of compressively strained germanium tin ($Ge_{1-x}Sn_x$) semiconductor epilayers, grown by chemical vapor deposition on a standard Si(001) substrate, is demonstrated. Materials characterization results reveal unusual impact of dopants manifesting via a pronounced reduction of Sn content in the epilayer, accompanied by an enhancement of the growth rate, due to increasing p-type doping concentration. Furthermore, the opposite behavior for n-type doping is observed, resulting in a less pronounced increase of Sn concentration and no effect on growth rate. Nevertheless, a very high density of electrically active holes up to $\approx 4 \times 10^{20}$ cm^{-3} is obtained in p-type doped $Ge_{1-x}Sn_x$ epilayer resulting in the lowest resistivity of 0.15 mΩ cm among all in situ doped epitaxial and strained group-IV semiconductors. Also, the metal-to-insulator transition in $Ge_{1-x}Sn_x$ is experimentally demonstrated for doping levels above 1×10^{17} cm^{-3}, which is substantially lower than in any group-IV semiconductor, and theoretically predict it to be as low as $\approx 1 \times 10^{17}$ cm^{-3}. The findings enabled by the doping regime explored in this work can open novel prospects to engineer low resistivity contacts and charge current injection in applications covering next-generation transistors, qubits, diodes, electrically driven light sources, sensors and hybrid quantum devices.

1. Introduction

Novel group IV semiconductor heterostructures consisting of Silicon (Si), Germanium (Ge), and Tin (Sn), and epitaxially grown on Si or Silicon on Insulator (SOI) wafer are a natural way to improve the properties of modern state of the art Si semiconductor devices and to expand their existing functionalities. The semiconductor industry is one of the largest one in the World, with revenues of $555 billion industry in 2021.[1] Nowadays, Si is incorporated into the manufacture of over 99% of all semiconductor devices either as the wafer or the material used to grow the epilayers. Epitaxially grown Germanium Tin ($Ge_{1-x}Sn_x$) binary alloys have recently emerged as a versatile and promising semiconductor for a wide range of applications spanning fields such as microelectronics, photonics, spintronics, and quantum technologies.[2] These group IV materials offer the possibility to leverage strain and bandgap engineering to tune device performance and to embed optimized components into conventional Si-based integrated circuits. $Ge_{1-x}Sn_x$ is expected to be an essential building block to implement source/drain contacts in future high-performance field-effect transistors,[2c,3] qubits, and low-resistivity ohmic contacts in large variety of devices spanning from diodes, including light emitting devices (LEDs), lasers, etc. up to sensors. Heavily doped $Ge_{1-x}Sn_x$ epilayers, with electrically active dopants, can act as stressors to enhance carrier mobility and simultaneously serve as suitable contacts for efficient injection of electrical current. The latter property is a key enabling factor also in electrically pumped lasers, LEDs, modulators, and photodetectors. The electrically pumped laser has been reported only very recently in $Ge_{1-x}Sn_x$ and proved severely limited to low-temperature operation.[2o,4] Contact engineering is thus one of the critical aspects that need to be advanced to bring $Ge_{1-x}Sn_x$ photonics, electronics, and sensors a step closer to real-life deployment. It is worth noting that heavily doped $Ge_{1-x}Sn_x$ alloys are also endowed with plasma frequencies in the mid- and far-infrared ranges of the electromagnetic spectrum. This is a yet-untapped feature that could lead to novel optical technologies based on plasmonic sensors with distinct advantages in diverse fields including point-of-care diagnostics and light harvesting for photovoltaics.[5] Finally, tailored carrier mobilities and electrical conductivities in highly doped materials are a steppingstone in maximizing the energy conversion efficiency for waste heat recovery. Efforts on this subject can arguably

M. Myronov, P. Jahandar
Department of Physics
The University of Warwick
Coventry CV4 7AL, UK
E-mail: M.Myronov@warwick.ac.uk
S. Rossi, F. Pezzoli
Dipartimento di Scienza dei Materiali
Università degli Studi di Milano-Bicocca
LNESS and BiQuTe, via R. Cozzi 55, Milano I-20125, Italy
K. Sewell, F. Murphy-Armando
Tyndall National Institute
University College Cork
Cork T12R5CP, Ireland

The ORCID identification number(s) for the author(s) of this article can be found under https://doi.org/10.1002/aelm.202300811

DOI: 10.1002/aelm.202300811

Table 1. Summary of the variable materials parameters of the strained $Ge_{1-x}Sn_x$/Ge/Si(001) heterostructures. The $Ge_{1-x}Sn_x$ epilayer's thickness, Sn content, and lattice mismatch strain are measured at 293 K. Carrier density, sheet resistivity, and resistivity are all data obtained with Hall effect and resistivity measurements at 15 K.

ID	$Ge_{1-x}Sn_x$ thickness [nm ± 0.5]	Sn content [% ± 0.1]	Lattice mismatch strain [%]	Carrier density [cm^{-3}]	Sheet resistivity [Ω/sq]	Resistivity [mΩ cm]	Dopant
p++	33	9.5	≈1.45	4×10^{20}	45	0.15	Boron
p+	30	10.6	≈1.62	3×10^{19}	115	0.35	Boron
p	27	11.6	≈1.77	1×10^{17}	29 940	81	Boron
n++	27	12.2	≈1.87	7×10^{19}	388	1.05	Phosphorus
n+	27	11.9	≈1.82	5×10^{19}	555	1.5	Phosphorus
n	27	11.6	≈1.77	1×10^{17}	64 057	173	Phosphorus
R	27	11.6	≈1.77	intrinsic	//	//	Undoped

disclose the full potential of $Ge_{1-x}Sn_x$ alloys in the burgeoning field of thermoelectrics and renewable energy.

Well-controlled incorporation and efficient activation of both donor and acceptor impurities in semiconductor $Ge_{1-x}Sn_x$ is indeed crucial for all the applications where charge transport plays a central role, let alone hybrid integration schemes in which the active region is based on III-V compounds rather than group IV materials. To this purpose, in situ doping through epitaxy of $Ge_{1-x}Sn_x$ films above the metal-to-insulator transition can provide a facile and effective method to yield low-resistivity ohmic contacts for a large variety of modern and future devices. In particular, only strained and heavily doped $Ge_{1-x}Sn_x$ epilayers, without additional defects generation, would lead to the highest electrical activity of dopants and therefore to the lowest material's electrical resistivity. Presently, however, little is known about electronic transport in epitaxial $Ge_{1-x}Sn_x$, especially under degenerate doping conditions. The available data often focus on one specific type of impurity, providing information within restricted temperature intervals, chiefly ≈300 K.[2l,6]

In this work we researched, both experimentally and theoretically, the p- and n-type in situ doping of strained, and therefore defect free, $Ge_{1-x}Sn_x$ epilayers and their impact on structural and electrical materials properties. Boron and phosphorus were used to as p- and n-type dopants, respectively.

2. Results and Discussion

2.1. Epitaxial Growth and Structural Characterization

Seven samples were grown (see Experimental Section for more details), *at unusually very low wafer's temperature of 260 °C and in hydrogen (H_2) carrier gas atmosphere*, with different doping levels of the $Ge_{1-x}Sn_x$ film: one undoped, as reference sample (R) with Sn content 11.6% ± 0.1 in the $Ge_{1-x}Sn_x$ alloy epilayer, three p-type doped using an increasing amount of boron (B) (p, p+, p++), and three n-type doped with phosphorus (P) (n, n+, n++). See **Table 1** for details. The doping range was varied between ≈1 × 1017 and over ≈1 × 1020 cm^{-3}. Diborane (B_2H_6) and Phosphine (PH_3) were used as precursors for p-type and n-type doping, respectively. The partial pressure of both precursors was the same for p and n, p+ and n+, and p++ and n++ samples. In contrast to most reported results, which stress the need of much more expensive and unstable Digermane (Ge_2H_6) diluted in H_2 as the precursor to grow epitaxial $Ge_{1-x}Sn_x$ thin films using Chemical Vapour Deposition (CVD), we used a standard Germane (GeH_4) precursor for Ge.[2i,6a,7] Also, in contrast to published results, the epitaxy takes place in a H_2 atmosphere, without nitrogen (N_2) presence.[2i,7] All samples were grown on prime grade 100 mm diameter on-axis p-Si(001) wafers with boron doping level in the range of 1–10 × 10^{15} cm^{-3}, at room temperature. The $Ge_{1-x}Sn_x$ epilayers are grown on ≈600 nm thick relaxed Ge buffer with low threading dislocation density and very smooth surface.[8] These relaxed Ge-on-Si heterostructures commonly serves as a template for the further deposition of binary $Ge_{1-x}Sn_x$ alloys. It has already enabled the successful exploration of various research questions, including the observation of photoluminescence from ultrathin $Ge_{1-x}Sn_x$ epilayers,[9] the demonstration of the first 2DHG in strained $Ge_{1-x}Sn_x$ QW,[2j,k] the investigation of spin coherent dynamics and lifetime in strained $Ge_{1-x}Sn_x$, as well as carrier dynamics in $Ge_{1-x}Sn_x$ epilayers.[2g,i] Such relaxed Ge buffers have been also utilized in the demonstration of mid-infrared light emission exceeding a 3 µm from strained $Ge_{1-x}Sn_x$ microdisks.[2e]

A schematic view of the samples is shown in the **Figure 1a**, while Table 1 summarizes each sample details, such as $Ge_{1-x}Sn_x$ epilayer thickness and Sn concentration obtained using HR-XRD. All epilayers thicknesses of $Ge_{1-x}Sn_x$/Ge/Si(001) heterostructures were obtained via analysis of XTEM images. Figure 1b shows a typical high magnification XTEM image of the surface region of one of the samples, with p+ 30 nm thick strained $Ge_{1-x}Sn_x$ epilayer and top region of very high-quality relaxed i-Ge buffer underneath.[8] The defect-free $Ge_{1-x}Sn_x$ epilayer with very smooth surface and abrupt interface between $Ge_{1-x}Sn_x$ epilayer and Ge buffer is clearly visible. Root mean square (RMS) surface roughness, measured by AFM, of all samples is ≈1 nm and does not change by either n- or p-type doping of the $Ge_{1-x}Sn_x$ epilayer. It means doping does not cause surface roughening, for example due to Sn clustering and segregation, and the measured surface roughness is due to relaxed Ge buffer layer only. Also, it indicates strong suppression of dopants segregation, in particular, phosphorus, by a very low wafer temperature.

Compressive strain in each $Ge_{1-x}Sn_x$ epilayer was confirmed by analyzing HR-XRD data. Representative high-resolution XRD ω–2θ scans for p-type and n-type samples are shown in **Figure 2a,b**, respectively. Here three major features can be observed. The rightmost peak, which is also the most intense, is

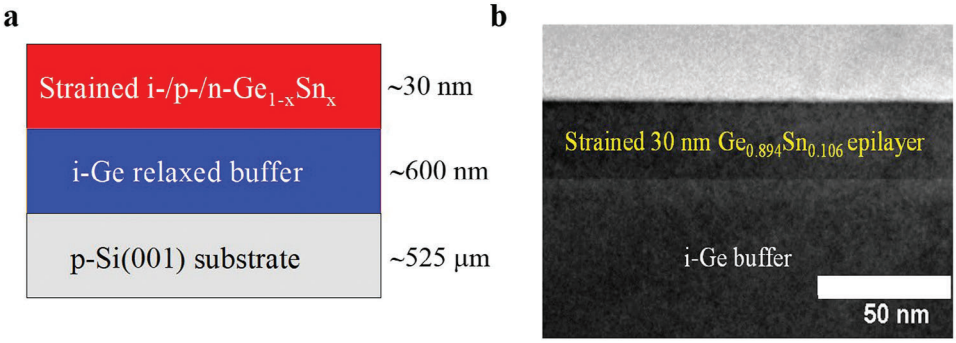

Figure 1. a) Schematics cross section of the strained $Ge_{1-x}Sn_x$/Ge/Si(001) heterostructures grown by CVD. b) High magnification XTEM image of the surface region of the p+ 30 nm thick strained $Ge_{1-x}Sn_x$ sample is shown.

attributed to the diffraction from the ≈525 μm thick lightly doped p-Si(001) substrate. At lower scattering angle of ≈33° the Ge Bragg peak from ≈600 nm relaxed Ge buffer is seen. Finally, the peaks at ≈32° are attributed to the compressively strained $Ge_{1-x}Sn_x$ alloy epilayers. Undoped, p and n reference samples have their $Ge_{1-x}Sn_x$ peaks at the same position, corresponding to Sn content of 11.6%. These peak shifts when the doping is increased, indicating a variation of the Sn content in the alloy. For p-type $Ge_{1-x}Sn_x$ epilayers, with higher boron doping, it shifts toward higher angles and Ge peak, indicating pronounced reduction in Sn content down to 10.6 and 9.5% for, p+ and p++ samples, respectively. In contrast, for n-type $Ge_{1-x}Sn_x$ epilayers with higher phosphorus doping the situation is opposite, but less pronounced. The peak shifts to lower angles and outward Ge peak indicating increase in Sn content up to 11.9 and 12.2% for, n+ and n++ samples, respectively. The fringes observed in the low angular region are due to X-ray interference and indicates the existence of strain in a $Ge_{1-x}Sn_x$ epilayer.

2.2. Temperature Dependent Hall Effect and Resistivity Measurements

Hall-bar devices, for subsequent electrical characterization of the samples using resistivity and Hall effect measurements over 15 – 300 K temperature range, were microfabricated using optical lithography, etching and contacts formation techniques. **Figure 3** shows a plan view optical image of a typical fabricated Hall-bar with width of 30 μm, spacing between potential contacts of 150 μm, and square contact pads with 125 μm side. Resistivity and Hall effect measurements were carried on such Hall-bars at the temperatures from ≈15 up to 300 K in a variable temperature cryostat and in darkness.

Before showing and explaining the obtained electrical characterization results it is necessary to note, with a reference to Figure 1a, that for the p-type samples the electrically active layers sequence at room temperature, in vertical direction, of the $Ge_{1-x}Sn_x$/Ge/Si(001) heterostructures appears to be p-i-p structure and for n-type samples it is n-i-p structure. However, due to the nature of Ge semiconductor material there are some thermally activated carriers, at the level below ≈10^{16} cm^{-3}, in the Ge relaxed buffer layer at room temperature. Therefore, for the p- and n-type samples it will correspond to the p-n(p)-p and n-n(p)-p structures, respectively. However, with reduction of temperature, the carriers in the lightly doped p-Si(001) substrate and Ge buffer layers are expected to freeze out, and at temperatures below ≈100 K they become insulator-like with no electrical conduction via them.[10] As a result, electrical conductance will occur via the $Ge_{1-x}Sn_x$ epilayer only and measured resistivity and Hall coefficient will correspond to intrinsic properties of either holes or electrons in the p- or n-type $Ge_{1-x}Sn_x$ epilayers, respectively. In contrast to these conditions, the higher temperature, including room temperature, the measurements will reveal some average resistivity and Hall coefficient of the $Ge_{1-x}Sn_x$/Ge/Si(001)

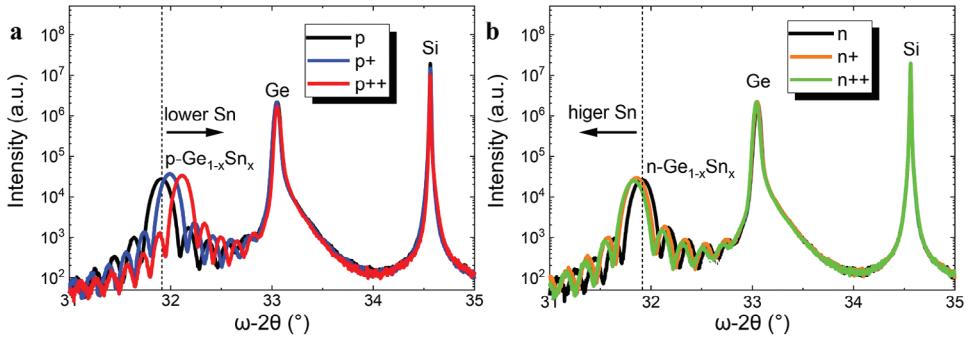

Figure 2. High-resolution XRD ω-2θ scans of a) p-type (Boron) and b) n-type (Phosphorus) doped strained $Ge_{1-x}Sn_x$ epilayers are shown. The well-defined interference pattern indicates the epilayer is fully strained while the position of the main peak at ≈32°, for each spectrum, is related to the Sn content in the $Ge_{1-x}Sn_x$ alloy.

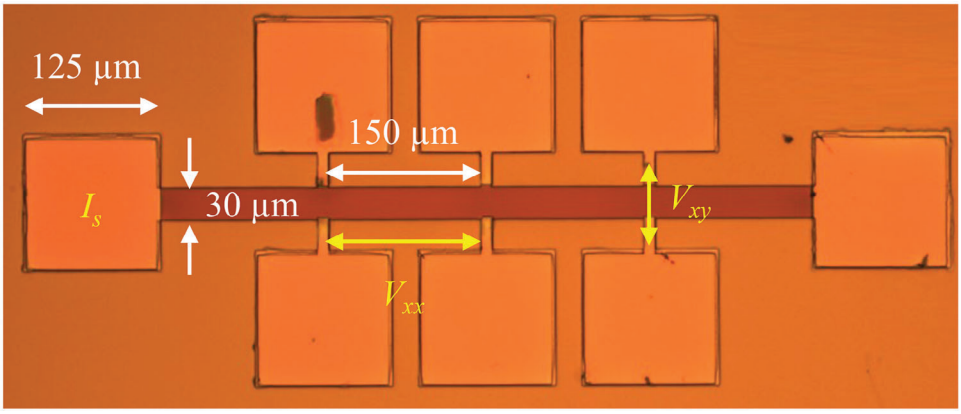

Figure 3. Optical image of the Hall-bar patterned via lithographic process. The width of the Hall bar is 30 µm and a distance between nearest potential contacts (V_{xx}) is 150 µm. Hall voltage (V_{xy}) is measured across the bar opposite contacts, as shown.

heterostructure. In particular, it results in substantial overestimation of electrically active carrier density in the doped $Ge_{1-x}Sn_x$ epilayer, as can be seen in **Figure 4**.

Figure 4a,b summarizes the measured transport data as a function of temperature for the p-type samples. Let us focus, at first, on the p-doped sample that have the lowest doping concentration.

The temperature dependence of ρ_{xx} can be suitably divided into two well-defined regimes. As the temperature decreases from room temperature to ≈225 K, ρ_{xx} rises sharply by about three orders of magnitude, e.g., from 27 to 13 100 Ω sq^{-1}. To gather a better understanding of these findings we can consider that $Ge_{1-x}Sn_x$/Ge heterostructures grown on Si are inherently multilayered since the insertion of the intrinsic Ge buffer is unavoidable as it mitigates the large lattice mismatch between $Ge_{1-x}Sn_x$ and the Si substrate, see Figure 1. The increasingly reduced bandgap of these materials (see **Figure 5a**) suggests that carriers are favorably located in the $Ge_{1-x}Sn_x$ layer; however, temperature can play a crucial role and activate carriers in underneath layers. We therefore expect that the suppression of the parallel conduction/charge contribution from the substrate is important to gather access to the intrinsic transport properties of the epitaxial $Ge_{1-x}Sn_x$ alloy. Indeed, despite the doping being in the top $Ge_{1-x}Sn_x$ layer, free charges due to the background doping of the Ge-on-Si substrate (see schematic in Figure 5b), can be non-negligible as the thickness, and therefore volume of the underneath layers, are orders of magnitudes thicker/larger that of the $Ge_{1-x}Sn_x$ thin film epilayer. According to this physical picture, the steep rise of the ρ_{xx} observed in our data (Figure 4a) can be intuitively ascribed to the thermal freezing of the charge reservoir offered by the Ge-on-Si buffer. A further support to this interpretation is obtained by an Arrhenius fit of ρ_{xx}, which in this temperature range gives for both n- and p-type samples a slope of ≈675 meV. Such a value is large for traps and is strikingly comparable with the average Ge bandgap in that temperature range.[11] On the contrary, below 225 K a much lower rise occurs: ρ_{xx} increases by less than three times as the temperature approaches 15 K.

The suppression of the charge contribution from the underneath Ge-on-Si layers is responsible also for the strong reduction of the Hall sheet density (p_{Hall}), which varies from ≈2 × 1014 cm^{-2} at 300 K to 6 × 1011 cm^{-2} at 225 K for both p- and n-dopants. p_{Hall} summarized in Figure 4b demonstrates a modest twofold decrease as the temperature is further reduced from 225 to 15 K. The almost constant Hall sheet density is a feature typical of metal-like materials, thus suggesting that the evaluated doping level of 1017 cm^{-3} in 27 nm thick $Ge_{0.883}Sn_{0.117}$ epilayer is enough to achieve the metal-to-insultation transition within $Ge_{1-x}Sn_x$.[12] The strict definition of MIT entails the presence of conduction at any temperature. This, in turn, implies that the activation energy of the donors or acceptors is less than or equal to zero [see, e.g.,[12a]]. In this work, we provide compelling experimental evidence to demonstrate that these conditions are

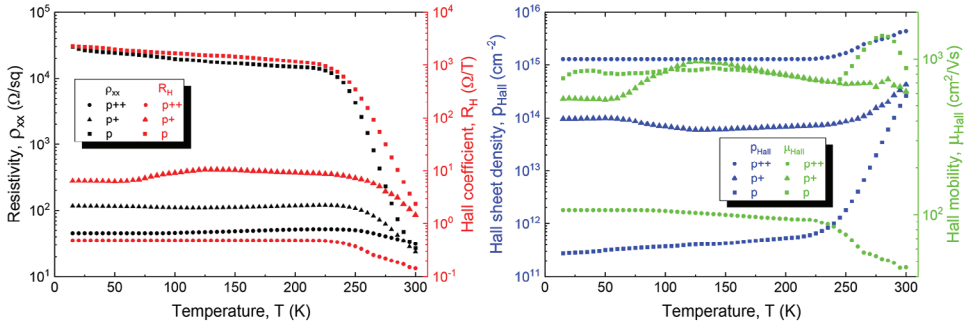

Figure 4. a) Sheet resistivity and Hall coefficient as a function of temperature for p-type doped samples. b) Hall sheet carrier density and Hall mobility as a function of temperature for p-type samples.

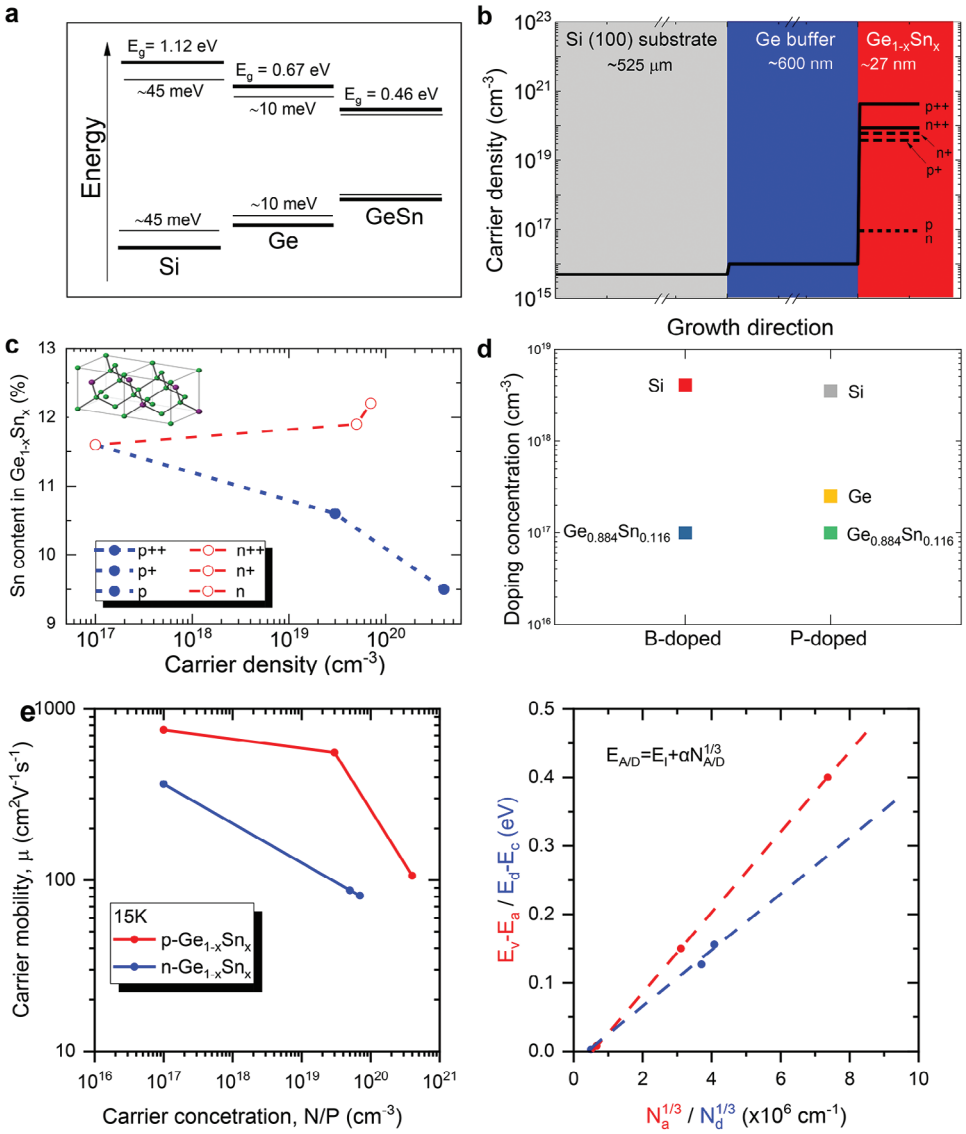

Figure 5. a) Simple schematic reporting the energy gap for unstrained low-doped materials and dopants activation energy for Si and Ge.[24] For $Ge_{1-x}Sn_x$/Ge no available data have been found in literature. Using First principles GW calculations, we calculate an indirect gap for strained $Ge_{1-0.12}Sn_{0.12}$/Ge of 0.54 eV at 0K, expected to reduce to 0.46 eV at room temperature. The band offsets depend on the doping, so they are ignored in this sketch. b) Schematic of the carrier density of a sample at room temperature. Black lines are for B (P) doping. Straight lines are for highest doped samples, dashed lines for the intermediate doped samples and dotted lines for the lowest doped samples. c) Low temperature results of Sn content for both p-type (solid dots) and n-type (empty triangles) doped samples as a function of the Hall carrier density at 15 K. Insert shows crystal structure of the $Ge_{1-x}Sn_x$ binary alloy d) Doping concentration required for the metal-to-insulation transition for Si:P[15] (3.5×10^{18} cm^{-3}), Si:B[16] (4×10^{18} cm^{-3}), Ge:P[17] (2.5×10^{17} cm^{-3}), $Ge_{0.084}Sn_{0.116}$:P (this work), and $Ge_{0.883}Sn_{0.116}$:B (this work) materials. e) Carrier mobility as a function of carrier concentration in n- and p-type $Ge_{1-x}Sn_x$ epilayers measured at 15 K. f) Activation energy of acceptors (red) and donors (blue) versus doping concentration. The doping concentrations and activation energies were obtained by fitting the calculated carrier concentration versus T to our experimental measurements (such as that in Figure 4b). The dashed lines show a fit with Equation (1), yielding $\boldsymbol{E_I} = 31\ \boldsymbol{meV}$ and $\boldsymbol{\alpha} = 5.85 \times 10^{-8} \frac{\boldsymbol{cm}}{\boldsymbol{eV}}$, with the MIT at 1.6×10^{17} cm^{-3} for holes, and yielding $\boldsymbol{E_I} = 19\boldsymbol{meV}$ and $\boldsymbol{\alpha} = 4.13 \times 10^{-8} \frac{\boldsymbol{cm}}{\boldsymbol{eV}}$, with the MIT at 9.6×10^{16} cm^{-3} for electrons.

fully met. Again, the similarity between the p and n samples suggests that the contribution due to the carrier conduction from the Ge-on-Si increases above 225 K. Figure 4a shows for the heavily doped $Ge_{1-x}Sn_x$ epilayers, i.e., p++ sample a pronouncedly reduced temperature dependence of ρ_{xx} compared to the p sample As expected, at low temperatures, ρ_{xx} is reduced by almost 3 orders of magnitude compared to the less doped materials (p) and their temperature dependence is much reduced, changing from 30 Ω sq^{-1} at 300 K to 45 Ω sq^{-1} at 15 K for the p++ sample. From the Hall sheet carrier density data as well as from the measurements of the Hall mobility (μ_{Hall}) reported in Figure 4b, we notice that the conduction demonstrates a small dependence on the temperature, which can be primarily ascribed to the thermal loss of carrier energy. Indeed, p_{Hall} varies from ≈4×10^{15} cm^{-2} at

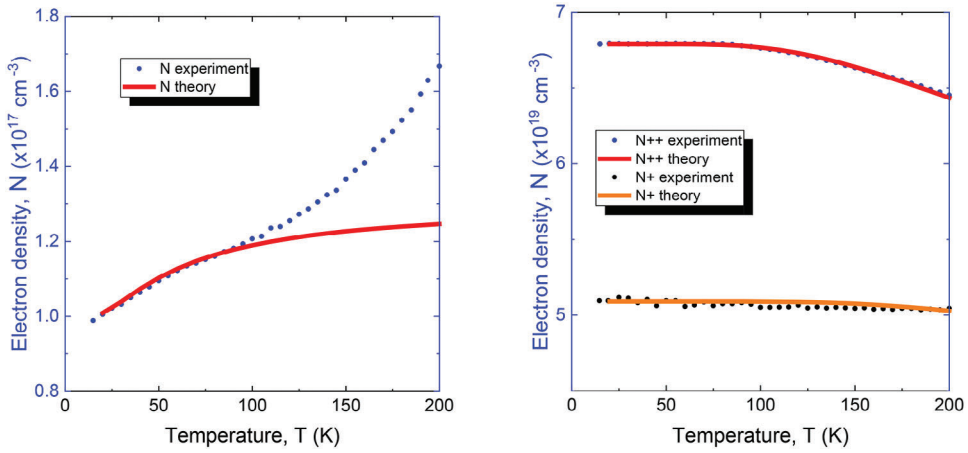

Figure 6. Measured (dots) and theoretical modeling (solid line) of the n-type carrier density vs temperature for the n (left), n+ and n++ (right) samples. The theoretical curves are calculated using first-principles methods to obtain the electronic structure as seen in the Experimental Section. From these curves we determine the density of donor impurities and the ionization energy. The departure of the theoretical curve from the experimental curve at 100 K in the left figure occurs due to the influx of carriers from the substrate into the $Ge_{1-x}Sn_x$ epilayer.

300 K to ≈1×10^{15} cm^{-2} at 15 K for p++ sample. At the same time μ_{Hall} increases from ≈45 up to ≈105 cm^2 Vs^{-1}, while the temperature changes from 300 K down to 15 K. It is necessary to note that for the p++ sample the Hall mobility increase rapidly while temperature decreases from the 300 K down to 225 K and then remains almost constant. The temperature independence of the transport properties indicates existence of a metal-like conduction in the heavily doped epilayers. But in our case, it can be observed not only in these heavily doped materials, but also in the less-doped ones. Figure 4 further clarifies that the freeze out of the Ge-on-Si shunt does not significantly affect the transport occurring in the p++ $Ge_{1-x}Sn_x$ epilayer, as opposed to the insulator-like behavior of the less doped p epitaxial layer.

Due to the activation of parallel conduction channels via p-Si substrate and the Ge buffer at high temperatures we are unable to properly estimate the Hall carrier density throughout the whole temperature range. We can safely limit our estimation to the case of 15 K where the conduction is expected to happen in the $Ge_{1-x}Sn_x$ layer only. In this case we obtain a Hall carrier density of 4 × 1020 cm^{-3} for p++ and 7 × 1019 cm^{-3} for n++, and ≈1 × 1017 cm^{-3} for p and n samples. This doping level is consistent with a complete activation of the dopants introduced. Analysis of partial pressure of B_2H_6 dopant precursor on the carrier density shows linear dependence from the lowest to the maximum values. It leads us to the conclusion that the limit for B incorporation into the $Ge_{1-x}Sn_x$ epilayer matrix has not been achieved. As a result, higher carrier density, i.e., above 4 × 1020 cm^{-3}, could be achieved by further increasing B_2H_6 partial pressure. In contrast to p-type doping, n-type doping using P in strained $Ge_{1-x}Sn_x$ epilayer is limited to much lower values, i.e., 7×10^{19} cm^{-3}. Similar phenomenon is observed for n-type doping of Si, SiGe, and Ge epilayers. As we shall see later, this seems to be due to less favorable absorption of n-type dopants in the group IV material, either because of their large size or reasons yet to be determined. The behavior of carrier density versus temperature, shown in **Figure 6**, and activation energy versus carrier density, shown in Figure 5, is consistent with this hypothesis, as the agreement between the measured density and the first-principles theoretical model is excellent in the range of temperatures where the contribution from substrate electrons is minimal. The agreement with the theoretical model indicates that the number of carriers in the conduction band is entirely determined by the density of states of the conduction band and the dopant density.

Figure 5c demonstrates effect of both p- and n-type doping on the formation of the $Ge_{1-x}Sn_x$ solid solution. The same growth conditions were maintained for all the samples, including partial pressure of $SnCl_4$ and GeH_4 gas precursors. No changes in Sn content are observed between the undoped $Ge_{1-x}Sn_x$ and both p- and n-doped up to relatively low values of 10^{17} cm^{-3}. N-type doping with PH_3 leads to slight increase in Sn content from 11.6%, for undoped reference sample and low doped n (1×10^{17} cm^{-3}), up to 11.9% for n+ (5×10^{19} cm^{-3}) and additionally to 12.2% for n++ (7×10^{19} cm^{-3}) samples. In contrast, p-type doping with diborane leads to pronounced changes in Sn content manifested itself via reduction of Sn content down to 10.6% for p+ (3×10^{19} cm^{-3}) and 9.5% for p++ (4×10^{20} cm^{-3}) samples. A similar phenomenon has been reported before for lower Sn content (≈7% in undoped) $Ge_{1-x}Sn_x$ epilayers characterized at room-temperature only.[13] Also, this finding is in line with previous literature reports on B doped $Ge_{0.93}Sn_{0.07}$ multilayers, where it was suggested that a surface-site competition between B and Sn can be the cause of a lower Sn incorporation.[14] However, we believe it is due to chemical reaction between B_2H_6 and $SnCl_4$ in gas phase. In contrast to reported hypotheses, we believe the observed changes do not lead to creation of ternary alloys, like $Ge_{1-x}Sn_{1-x-y}B_y$. Insert of Figure 5c shows a crystal structure of the $Ge_{1-x}Sn_x$ binary alloy. Electrically active doping in a semiconductor crystal is achieved by a substitutional incorporation of dopant atom into a crystal structure. In the case of $Ge_{1-x}Sn_x$ it means B or P can either occupy Ge or Sn sites. Hypothetically, a ternary $Ge_{1-x}Sn_{1-x-y}B_y$ or $Ge_{1-x}Sn_{1-x-y}P_y$ alloy could be synthesised if the carrier density, i.e electrically active doping level, of either B or P will be well above ≈5×10^{20} cm^{-3}. In our case we already observed reduction of Sn content by 1% in the $Ge_{1-x}Sn_x$ alloy with B doping just. 3×10^{19} cm^{-3}. Even doping with the highest

partial pressure of B_2H_6 does not lead to incorporation of even of 1% of B (4×10^{20} cm^{-3} for p++ sample) into the lattice structure of $Ge_{1-x}Sn_x$ binary alloy. And therefore, cannot be responsible for creation of ternary $Ge_{1-x}Sn_{1-x-y}B_y$ alloy. However, weaker B—B bonds of the B_2H_6 are easily broken by Cl species from $SnCl_4$ molecules decomposition, even at this extremely low temperature of 260 °C for epitaxy. Also, it could be a reason for the neutralization of some Sn molecules by B ones in the gas phase, leading to a reduction of Sn in the gas phase and therefore less Sn incorporation in the alloy with addition of the B_2H_6 precursor. Further research is needed to identify what is the critical B_2H_6 partial pressure that is responsible for this effect. For now, we see it could be in a range which corresponds to the carrier density between $\approx 5 \times 10^{17}$ and $\approx 5 \times 10^{18}$ cm^{-3}. This behavior also explains why the epilayer's thickness increases with increasing B doping. It occurs because for selected growth conditions, the growth rate increases with a reduction of Sn content in the $Ge_{1-x}Sn_x$ epilayer. This effect is not visible for the n-type samples doped with P due to the much stronger binding energy between P and Hydrogen in the PH_3 precursor. In contrast to the reduction of Sn content in the $Ge_{1-x}Sn_x$ epilayer with B_2H_6 doping, a slight increase of Sn content in n-type doped samples is observed. At the same time the growth rate does not change with a slight increase in the Sn content, which becomes clearly visible for higher PH_3 partial pressure only. Because either doping with B_2H_6 or PH_3 achieves very high levels of electrically active dopants up to either 4×10^{20} cm^{-3} or 7×10^{19} cm^{-3}, respectively, it means dopants occupy substitutional sites in the crystal lattice of the $Ge_{1-x}Sn_x$. Further research is essential to understand which sites are occupied by B and which are by P. Either of them could displace either Sn or Ge atoms. But in any case, it does not lead to formation of $Ge_{1-x}Sn_{1-x-y}B_y$ ternary alloy responsible for over 2% reduction in Sn content for B doped $Ge_{1-x}Sn_x$ epilayer. Increase in Sn content by 0.5% for P doped $Ge_{1-x}Sn_x$ epilayer is not responsible for formation of the $Ge_{1-x}Sn_{1-x-y}P_y$ ternary alloy either. Additionally, there is a need to validate the maximum achievable doping level incorporation in the $Ge_{1-x}Sn_x$ epilayers as a function of Sn content, etc. Moreover, we intentionally designed this experiment with fully strained $Ge_{1-x}Sn_x$ epilayer of very high Sn content of ≈12% because strain relaxation of $Ge_{1-x}Sn_x$ is very unusual from other semiconductors and leads to the emergence of various effects, including substantially higher Sn incorporation into $Ge_{1-x}Sn_x$ epilayer with strain relaxation, roughening the surface, appearance of defects etc. All these effects unavoidably will result in changes in both p- and n-type dopants incorporation in the $Ge_{1-x}Sn_x$ epilayer.

In Figure 5d we show the doping level required to achieve a metal-to-insulator transition for doped Si and Ge, i.e., Si:P,[15] Si:B,[16] and Ge:P.[17] We have also included the results for both strained $Ge_{0.884}Sn_{0.116}$:P and $Ge_{0.884}Sn_{0.116}$:B that we obtained from our the lowest doped samples, i.e., p and n. Despite the lack of literature data for Ge:B it is reasonable to expect a reduction of the required doping to observe the crossover by alloying Ge with Sn. The only work addressing the metal-to-insulator transition (MIT) in Ge:B is[18] In this work, the MIT is found to be between 1.5×10^{17} and 1.15×10^{19} cm^{-3}. A monotonic reduction of the required doping is visible from Si to Ge. The (MIT) in semiconductors depends on the interaction of the impurity ions and the carrier density with the valence or conduction bands,[19] and occurs at the meeting of the impurity activation energy with the conduction or valence band, following the relation

$$E_{A/D} = E_I + \alpha N_{A/D}^{1/3} \quad (1)$$

where $E_{A/D}$ is the activation energy of the (A)cceptor or (D)onor, E_I is the ionization energy of the impurity, $N_{A/D}$ is the concentration of acceptors or donors and α is a constant that depends on the screening of the impurities by the free carriers in the conduction or valence bands, and is determined here by fitting (see Figure 5f).

The higher MIT on Si relative to Ge can be ascribed to the closer positioning of the dopants level (≈10 meV) in Ge to the corresponding band with respect to Si (≈45 meV) and a shallower slope α in Equation (1). The lower dopants activation energy results in achieving MIT at lower doping level, promoting all dopants to either conduction or valence band edges in case of either n- or p-type doping, respectively. Despite the lack of information regarding the positioning of the dopants level in $Ge_{1-x}Sn_x$, we have used our measured Hall densities to calculate E_I and α and find that they indeed have a steeper slope than Ge, albeit slightly deeper ionization energies (See fit in Figure 5f). Consequently, we expect the MIT to occur at lower doping than in Ge. Our experimental results are marked with a dashed arrow indicating that we leave open the precise positioning of the metal-insulator threshold. With the measured Sn content, we theoretically predict the MIT in lightly doped samples by calculating the doping energy level crossing of the conduction band. This transition turns out to be reached at 9.6×10^{16} cm^{-3}, in line with the limiting range pointed out by the experimental result. However, it will require further validation via an experiment.

Figure 5e summarises carrier mobility as a function of carrier concentration in n- and p-type $Ge_{1-x}Sn_x$ epilayers measured at 15 K. In both cases the mobility of either holes or electrons reduces with increasing carrier concentration due to increasing carriers scattering on ionised impurities, in our case either B or P. But it is interesting to note that hole mobility in strained $Ge_{1-x}Sn_x$ is higher than electron mobility in the obtained range of carrier density. Usually, electron mobility is higher than hole one in any bulk or relaxed semiconductor. We think our results could be explained by presence of compressive strain in the epilayer, which is responsible for the enhancement of hole mobility. Most likely it is due to a reduced effective mass. Recently, the first measurements of holes effective mass in strained $Ge_{1-x}Sn_x$ quantum well (QW) revealed its very low value down to 0.09 m*.[2k] The only lower hole effective mass is observed in strained Ge QW.[20] Also, the reduced effective mass most likely is responsible for relatively high Hall hole mobility of 106 cm^2 V^{-1} s^{-1} at the highest carrier density of $\approx 4 \times 10^{20}$ cm^{-3}. It is almost double the Hall hole mobility reported before, for $Ge_{1-x}Sn_x$ epilayers doped with B up to $\approx 3 \times 10^{20}$ cm^{-3} and grown by CVD at 350 °C.[14]

We now elaborate a bit further on the resistivity measurement of our materials. First from the low temperature, at 15 K, data we calculated the resistivity of the material. The results are shown in Table 1. For p++ and n++ resistivity of 0.15 and 1.05 mΩ cm are obtained, respectively. This difference is explained by limited P dopants incorporation comparing to B ones at the same partial pressure and therefore lower carrier density, i.e., $\approx 7 \times 10^{19}$ cm^{-3} comparing to $\approx 4 \times 10^{20}$ cm^{-3}. It is necessary to note that obtained

electrical resistivity of 0.15 mΩ cm, for the highest B doped at ≈4×10^{20} cm^{-3} $Ge_{1-x}Sn_x$ strained epilayer, is the lowest among all group IV semiconductors, including previous attempts in doping of $Ge_{1-x}Sn_x$ epilayers.[6a,13,14,21]

It should be noted that our work does not impose limitations on the applicability of $Ge_{1-x}Sn_x$ epilayers in the high temperature regime. In fact, our findings are valuable for discriminating the specific transport contribution from $Ge_{1-x}Sn_x$ in complex heterostructures composed of multiple junctions. Moreover, the electrical parameters we derived in our work are also central for modeling and designing applications in which $Ge_{1-x}Sn_x$ devices operate at room temperature and above. The insights gained from our work are thus relevant and beneficial for physicists interested in fundamental transport mechanisms as well as engineers interested in device applications covering a wide range of temperature conditions.

Obtained results clearly demonstrate a huge potential of efficient uniform doping of $Ge_{1-x}Sn_x$ epilayers, essential for many devices technologies, including lasing, and realization of novel hybrid devices concepts, including quantum devices.[22] In particular, for now, p-type doping of $Ge_{1-x}Sn_x$ leads to the lowest resistivity, comparing to the same carrier concentration, among all group IV semiconductors including Si, $Si_{1-x}Ge_x$, Ge, SiC, and Diamond. It is explained by efficient doping, leading to full electrical activation of dopant impurities and relatively high mobility, despite the lowest epitaxial growth temperature among any group-IV semiconductor material. Lower bandgap of the $Ge_{1-x}Sn_x$ semiconductor material is additionally reduced by the presence of compressive biaxial strain in it.

Moreover, obtained resistivity values are the lowest even comparing to other materials technologies including group III-V semiconductors, carbon nanotubes, graphene and other 2D materials. It is necessary to stress that typical growth temperature of $Ge_{1-x}Sn_x$ epilayers by CVD using either GeH_4 or Ge_2H_6 and $SnCl_4$ precursors is in the range of ≈ 300 – 350 °C.[21] We were able to substantially reduce it even down to 260 °C, for high Sn content $Ge_{1-x}Sn_x$ epilayers. Therefore, very low-growth temperature makes $Ge_{1-x}Sn_x$ material even more attractive as a backend process for formation of low resistivity ohmic contacts, via blanket or selective area epitaxy, in semiconductor devices fabricated of know and emerging semiconductor materials, because it suppresses a diffusion and strain relaxation in underlaying materials. Overall, it makes the doped $Ge_{1-x}Sn_x$ epilayers the best contact materials for various devices technologies and will not only be limited to the group IV semiconductors, but also could be epitaxially grown on other monocrystalline semiconductors with appropriate lattice structure and range of suitable in plane lattice constants, including for an example GaAs, InGaAs and many others.

3. Conclusion

In conclusion, in situ doping of compressively strained $Ge_{1-x}Sn_x$ epilayers, grown by CVD, at very low substrate temperature of 260 °C, reveals unusual impact of dopants manifesting via a pronounced reduction of Sn content in the epilayer accompanied with enhancement of growth rate, due to increasing p-type doping concentration and the opposite behavior for n-type doping, but resulting in a less pronounced increase of Sn concentration and no effect on growth rate. Very high carrier density of holes up to ≈4×10^{20} cm^{-3} is obtained in p-type doped $Ge_{1-x}Sn_x$ epilayer resulting in the lowest resistivity of 0.15 mΩ cm among all in situ doped epitaxially and strained group-IV semiconductors. In contrast to p-type doping, n-type doping using P in strained $Ge_{1-x}Sn_x$ epilayer is limited to much lower values, i.e., 7×10^{19} cm^{-3}. Therefore, efficient p- and n-type doping of $Ge_{1-x}Sn_x$ epilayers in the range between ≈10^{17} and ≈4×10^{20} $cm^{-3}$is demonstrated. Substantially lower, than in any group-IV semiconductor, the MIT in $Ge_{1-x}Sn_x$ for doping levels above ≈1×10^{17} cm^{-3} is observed. Our findings can contribute to the development of efficient current injection in future electronic devices, thus facilitating the transition of technologies and heterostructures based on $Ge_{1-x}Sn_x$ from research labs to the industrial production.

4. Experimental Section

Epitaxial Growth of $Ge_{1-x}Sn_x$ Heterostructures: The growth was performed in a reduced pressure chemical vapor deposition (RP-CVD) system ASM Epsilon 2000, while the chamber was kept in H_2 atmosphere, by introducing Tintetrachloride ($SnCl_4$) and Germane (GeH_4) as gaseous precursors for the chemically- and thermally-induced deposition of the $Ge_{1-x}Sn_x$ epilayer. Diborane (B_2H_6) and Phosphine (PH_3) were utilized as precursors for the dopants. The $Ge_{1-x}Sn_x$ layers were epitaxially grown on 100 mm diameter Si(001) wafers via a non-intentionally doped relaxed Ge buffer layer. The $Ge_{1-x}Sn_x$ epilayer growth rate was 0.1 nm s^{-1}.

Structural Characterization: In plane and out of plain lattice constants of the $Ge_{1-x}Sn_x$ and Ge epilayers were obtained from analysis of ω–2θ scans and reciprocal space maps (RSM) obtained using Pan-analytical X'Pert Pro MRD diffractometer with CuKα radiation (λ = 0.15 418 nm). HR-XRD can quantify the crystal quality of the epilayer and assess whether the films are monocrystalline, polycrystalline, amorphous, and under significant levels of tilt or residual strain. The scan resolution was 0.0002 deg, which allows determination of Sn content in a $Ge_{1-x}Sn_x$ alloy with accuracy well above 0.01%. XTEM is one of the most effective techniques to assess the crystallinity, morphology, quality of epilayers and to measure the epilayer's thickness. XTEM micrographs were obtained on a JEOL 2100 TEM.

Fabrication of Hall Bars: $Ge_{1-x}Sn_x$ Hall bar devices were fabricated using optical lithography. The channel had a width of 30 µm and a length of 600 µm. The distance between contact pair for resistivity measurements was 150 µm. Contact metallization was performed via sputtering deposition of 100-nm-thick Pt layer on $Ge_{1-x}Sn_x$:B and a 150-nm-thick Au layer on $Ge_{1-x}Sn_x$:P. However, it was struggled to obtain ohmic contacts on $Ge_{1-x}Sn_x$ undoped material at low temperatures. All contact materials which had been tried so far exhibit Schottky behavior at low-temperatures. Without ohmic contacts Hall and resistivity data were unreliable and therefore could not be presented and discussed. Nevertheless, it was a topic of ongoing research and it was hoped to find a solution to this issue. The sputtered region of each contact covers an area of 125 × 125 μm^2. No annealing was needed on p+ and p++ samples since the *I–V* characteristics were ohmic in the whole temperature range, whereas annealing for 5 min at 200 °C in N_2 gas atmosphere was needed for all the other samples to avoid non-linear behavior of the *I–V* curves at cryogenic temperatures. A 5-min wet etching step in a solution of H_2O_2: NH_4OH: H_2O (1: 0.5: 80) for was performed to define a mesa with an approximate height of 300 nm.

Hall and Resistivity Measurements: Temperature dependent (15 – 300 K) measurements were performed in a variable temperature cryostat where a maximum magnetic field (B) of 0.5 T could be applied. A constant current (I_{xx}) of 1 µA was injected in the Hall bar while lock-in amplifiers measure the longitudinal (V_{xx}) and Hall (V_{xy}) voltage. The sheet resistivity (ρ_{xx}) was calculated as $V_{xx}/I_{xx} \times (W/L)$ where W is the width of the Hall-bar and L is the distance between a pair of side contacts (in these devices L = 5 W). The sheet carrier density (p_{Hall} or n_{Hall}) is obtained as $(B\ I_{xx})/(e\ V_{xy})$ where e is the electron charge. The carrier density was calculated as p_{Hall}/h or n_{Hall}/h where h is the $Ge_{1-x}Sn_x$ epilayer thickness. Finally, the Hall mobility (μ_{Hall}) was found as $1/(e\ p_{Hall}\ \rho_{xx})$ or $1/(e\ n_{Hall}\ \rho_{xx})$.

Theoretical Band Structure Calculations: The activation energies versus carrier concentration Figure 5 were obtained by fitting the activation energy in a first-principles-based calculation of the carrier density versus temperature for the various doping concentrations in this work. The carrier densities correspond to calculations of the band structure of GeSn based on DFT and GW calculations,[23] including the change in energy dispersion with temperature as calculated.[24] The carrier concentration based on the calculated band structure was obtained by

$$n_{v/c} = \sum_i \int d^3k\, f_i\left(E\left(k\right),\ E_F,\ T\right) \tag{2}$$

where f_i is the Fermi distribution corresponding to band i (the three valence bands or conduction L or Γ bands), that is a function of the crystal momentum k via the electronic energy dispersion $E(k)$. E_F and T correspond to the fermi level and temperature, respectively. The E_F is found by satisfying the condition

$$p_I + n_c = n_v + n_I \tag{3}$$

where p_I and n_I are the ionized hole and electron carrier densities, respectively, given by

$$n_I = \frac{N_D}{1 + 2\ Exp\left(\frac{E_F - E_D}{k_B T}\right)} \tag{4}$$

$$p_I = \frac{N_A}{1 + 4\ Exp\left(\frac{E_A - E_F}{k_B T}\right)} \tag{5}$$

where $E_{A/D}$ and the dopant concentrations $N_{A/D}$ were left as the only free parameters in the fitting of the magnitude of the carrier density versus T. The agreement of the calculated and measured temperature dependence of the carrier densities is excellent, except above the temperature of carrier activation in the Ge/Si substrate (>200 K), as shown in Figure 6.

Acknowledgements

The authors thank Dr Alan Burton for technical support of equipment and clean room facilities at Warwick University. F.M.A. acknowledges Science Foundation Ireland Frontiers of the Future award 19/FFP/6953. F.P. acknowledges support by the Air Force Office of Scientific Research under award number FA8655-22-1-7050.

Conflict of Interest

The authors declare no conflict of interest.

Data Availability Statement

The data that support the findings of this study are available on request from the corresponding author. The data are not publicly available due to privacy or ethical restrictions.

Keywords

CVD, doping, epitaxy, Germanium tin, metal-to-insulation transition

Received: November 20, 2023
Revised: June 16, 2024
Published online:

[1] https://www.semiconductors.org, (accessed: September 2021).
[2] a) S. Gupta, R. Chen, B. Magyari-Kope, H. Lin, Y. Bin, A. Nainani, Y. Nishi, J. S. Harris, K. C. Saraswat, presented at 2011 International Electron Devices Meeting, Washington, DC, USA, December **2011**. b) S. Wirths, A. T. Tiedemann, Z. Ikonic, P. Harrison, B. Hollander, T. Stoica, G. Mussler, M. Myronov, J. M. Hartmann, D. Grutzmacher, D. Buca, S. Mantl, *Appl. Phys. Lett.* **2013**, *102*, 192103; c) M. Liu, D. Yang, A. Shkurmanov, J. H. Bae, V. Schlykow, J.-M. Hartmann, Z. Ikonic, F. Baerwolf, I. Costina, A. Mai, J. Knoch, D. Grützmacher, D. Buca, Q.-T. Zhao, *ACS Appl. Nano Mater.* **2021**, *4*, 94; d) S. Wirths, R. Geiger, N. von den Driesch, G. Mussler, T. Stoica, S. Mantl, Z. Ikonic, M. Luysberg, S. Chiussi, J. M. Hartmann, H. Sigg, J. Faist, D. Buca, D. Gruetzmacher, *Nat. Photonics* **2015**, *9*, 88; e) R. W. Millar, D. C. S. Dumas, K. F. Gallacher, P. Jahandar, C. MacGregor, M. Myronov, D. J. Paul, *Opt. Express* **2017**, *25*, 25374; f) O. Moutanabbir, S. Assali, X. Gong, E. O'Reilly, C. A. Broderick, B. Marzban, J. Witzens, W. Du, S.-Q. Yu, A. Chelnokov, D. Buca, D. Nam, *Appl. Phys. Lett.* **2021**, *118*, 110502; g) S. De Cesari, A. Balocchi, E. Vitiello, P. Jahandar, E. Grilli, T. Amand, X. Marie, M. Myronov, F. Pezzoli, *Phys. Rev. B* **2019**, *99*, 035202; h) E. Vitiello, S. Rossi, C. A. Broderick, G. Gravina, A. Balocchi, X. Marie, E. P. O'Reilly, M. Myronov, F. Pezzoli, *Phys. Rev. Appl.* **2020**, *14*, 064068; i) E. Rogowicz, J. Kopaczek, J. Kutrowska-Girzycka, M. Myronov, R. Kudrawiec, M. Syperek, *ACS Appl. Electron. Mater.* **2021**, *3*, 344; j) Y. Gul, M. Myronov, S. N. Holmes, M. Pepper, *Phys. Rev. Appl.* **2020**, *14*, 054064; k) Y. Gul, S. N. Holmes, C. W. Cho, B. Piot, M. Myronov, M. Pepper, *J. Phys.-Condes. Matter* **2022**, *34*, 485301; l) S. Wirths, D. Buca, S. Mantl, *Prog. Cryst. Growth Charact. Mater.* **2016**, *62*, 1; m) N. von den Driesch, D. Stange, S. Wirths, D. Rainko, I. Povstugar, A. Savenko, U. Breuer, R. Geiger, H. Sigg, Z. Ikonic, J.-M. Hartmann, D. Grützmacher, S. Mantl, D. Buca, *Small* **2017**, *13*, 1603321; n) WirthsS, G. R., N. von den Driesch, MusslerG, S. T., MantlS, I. Z., LuysbergM, C. S., J. M. Hartmann, SiggH, F. J., BucaD, G. D., *Nat. Photonics* **2015**, *9*, 88; o) V. Reboud, D. Buca, H. Sigg, J. M. Hartmann, Z. Ikonic, N. Pauc, V. Calvo, P. Rodriguez, A. Chelnokov, in *Silicon Photonics Iv: Innovative Frontiers*, (Eds: D. J. Lockwood, L. Pavesi), Springer International Publishing, Cham **2021**; p) B. M. Ferrari, F. Marcantonio, F. Murphy-Armando, M. Virgilio, F. Pezzoli, *Phys. Rev. Res.* **2023**, *5*, L022035.
[3] A. M. Ionescu, H. Riel, *Nature* **2011**, *479*, 329.
[4] Y. Zhou, Y. Miao, S. Ojo, H. Tran, G. Abernathy, J. M. Grant, S. Amoah, G. Salamo, W. Du, J. Liu, J. Margetis, J. Tolle, Y. H. Zhang, G. Sun, R. A. Soref, B. Li, S. Q. Yu, *Optica* **2020**, *7*, 924.
[5] a) R. Soref, J. Hendrickson, J. W. Cleary, *Opt. Express* **2012**, *20*, 3814; b) S. Prucnal, F. Liu, M. Voelskow, L. Vines, L. Rebohle, D. Lang, Y. Berencén, S. Andric, R. Boettger, M. Helm, S. Zhou, W. Skorupa, *Sci. Rep.* **2016**, *6*, 27643.
[6] a) M. Frauenrath, V. Kiyek, N. V. Driesch, M. Veillerot, E. Nolot, D. Buca, J. M. Hartmann, *ECS J. Solid State Sci. Technol.* **2021**, *10*, 085006; b) H. Zhou, L. Zhang, J. Tong, S. Wu, B. Son, Q. Chen, D. H. Zhang, C. S. Tan, *Opt. Express* **2021**, *29*, 8498; c) A. Vohra, C. Porret, D. Kohen, S. Folkersma, J. Bogdanowicz, M. Schaekers, J. Tolle, A. Hikavyy, E. Capogreco, L. Witters, R. Langer, W. Vandervorst, R. Loo, *Jpn. J. Appl. Phys.* **2019**, *58*, SBBA04.
[7] P. Jahandar, D. Weisshaupt, G. Colston, P. Allred, J. Schulze, M. Myronov, *Semicond. Sci. Technol.* **2018**, *33*, 034003.
[8] a) V. A. Shah, A. Dobbie, M. Myronov, D. R. Leadley, *Solid-State Electron.* **2011**, *62*, 189; b) V. A. Shah, A. Dobbie, M. Myronov, D. R. Leadley, *Thin Solid Films* **2011**, *519*, 7911.
[9] F. Pezzoli, A. Giorgioni, D. Patchett, M. Myronov, *ACS Photonics* **2016**, *3*, 2004.
[10] a) M. Myronov, C. Morrison, J. Halpin, S. Rhead, C. Casteleiro, J. Foronda, V. A. Shah, D. Leadley, *Jpn. J. Appl. Phys.* **2014**, *53*, 04EH02; b) M. Myronov, Y. Shiraki, T. Mouri, K. M. Itoh, *Thin Solid Films* **2008**,

517, 359; c) M. Myronov, Y. Shiraki, T. Mouri, K. M. Itoh, *Appl. Phys. Lett.* **2007**, *90*, 192108.
[11] J. S. Blakemore, *Semiconductor Statistics*, Elsevier, Amsterdam **1962**.
[12] a) P. P. Debye, E. M. Conwell, *Phys. Rev.* **1954**, *93*, 693; b) H. V. Löhneysen, *Curr. Opin. Solid State Mater. Sci.* **1998**, *3*, 5; c) N. F. Mott, W. D. Twose, *Adv. Phys.* **1961**, *10*, 107.
[13] B. Vincent, F. Gencarelli, H. Bender, C. Merckling, B. Douhard, D. H. Petersen, O. Hansen, H. H. Henrichsen, J. Meersschaut, W. Vandervorst, M. Heyns, R. Loo, M. Caymax, *Appl. Phys. Lett.* **2011**, *99*, 152103.
[14] D. Kohen, A. Vohra, R. Loo, W. Vandervorst, N. Bhargava, J. Margetis, J. Tolle, *J. Cryst. Growth* **2018**, *483*, 285.
[15] a) C. Yamanouchi, K. Mizuguchi, W. Sasaki, *J. Phys. Soc. Jpn.* **1967**, *22*, 859; b) M. Hornung, A. Ruzzu, H. G. Schlager, H. Stupp, H. v. Löhneysen, *Europhys. Lett.* **1994**, *28*, 43.
[16] D. Belitz, T. R. Kirkpatrick, *Rev. Mod. Phys.* **1994**, *66*, 261.
[17] H. Fritzsche, *Phys. Rev.* **1962**, *125*, 1552.
[18] A. Ali, J. Singh, R. K. Gopal, *AIP Conf. Proc.* **2019**, *2115*, 030453.
[19] G. L. Pearson, J. Bardeen, *Phys. Rev.* **1949**, *75*, 865.
[20] a) C. Morrison, M. Myronov, *Appl. Phys. Lett.* **2017**, *111*, 192103; b) M. Myronov, J. Kycia, P. Waldron, W. H. Jiang, P. Barrios, A. Bogan, P. Coleridge, S. Studenikin, *Small Sci.* **2023**, *3*, 2200094.
[21] J. Aubin, J. M. Hartmann, J. P. Barnes, J. B. Pin, M. Bauer, *ECS J. Solid State Sci. Technol.* **2016**, *6*, P21.
[22] G. Scappucci, C. Kloeffel, F. A. Zwanenburg, D. Loss, M. Myronov, J.-J. Zhang, S. De Franceschi, G. Katsaros, M. Veldhorst, *Nat. Rev. Mater.* **2021**, *6*, 926.
[23] X. Gonze, *Z. Kristallogr. – Cryst. Mater.* **2005**, *220*, 558.
[24] F. Murphy-Armando, *J. Appl. Phys.* **2019**, *126*, 215103.